

CONSTRUCTION OF VASCULAR GRAFT BY 3D PRINTING USING BACTERIAL CELLULOSE FORMULATION AS BIOINK

NEVRA PELIN CESUR and NELISA TÜRKÖĞLU LAÇİN

Molecular Biology and Genetics Department, Yıldız Technical University, Istanbul, Turkey

✉ *Corresponding author: N. Türkoğlu Laçin, nelisalacin@gmail.com*

Received October 15, 2021

Currently, there is a considerable clinical demand for biocompatible and robust tissue-engineered artificial vascular graft materials. The vascular application requiring adequate mechanical strength and biocompatibility still lags at some critical points. Bacterial cellulose (BC) is well known for its use as a biomaterial in various fields due to its high biocompatibility. The most critical issue preventing the wide use of BC for 3D biomaterial printing is its insolubility in water and organic solvents. Because of this feature, the use of BC as bioink is limited. In this study, optimizing the solubility of BC with zinc sulphate, and the application of the obtained bioink with a 3D printing technique to create a model vascular graft, as well as examining it in terms of mechanical strength, were carried out for the first time in the literature.

The chemical characterization of the obtained vascular graft was performed by FTIR, RAMAN and SEM analyses. The thermal behavior was analyzed by TG analysis (showing mass losses of 22.72% at 361 °C and 52.4% at 421 °C). The surface area was measured as 8.290 m²/g. The water retention capacity (WRC) was examined throughout 48 hours (after 1 h – 5%, 24 h – 9%, and 48 h – 9%). The elasticity modulus of the sample was 172.083 N/mm² and the elongation break was 87.591%. The cytotoxicity analysis results revealed that cell viability reached 75.84% on the only resin-containing 3D-printed aorta, while it was 100% on the BC/zinc sulfate-resin composite 3D-printed aorta. The morphology of the human umbilical vein endothelial cells (HUVECs) was observed after 24, 52 and 72 h. Cell adhesion to the BC-based composite 3D printed vascular graft was determined as 89.02% after 24 h, 92.01% after 52 h, 100% after 72 h, while it reached much lower values for the only resin-containing 3D vascular graft – of 55.02% after 24 h, 56% after 48 h, and 58.04% after 72 h. Additionally, the rheological analysis indicated that the yield stress of the BC-based bioink increased with the BC content up to 20 Pa.

Keywords: 3D printing, patient-specific vascular graft, tissue engineering

INTRODUCTION

The worldwide demand for organ replacement or tissue regeneration is increasing. The tissue engineering is generally based on scaffolds to provide sufficient support for cell attachment, proliferation and differentiation. Considering some challenges, such as rejection of the biomaterials used and inflammation caused by them, recent tissue engineering and regenerative medicine studies have focused on 3D printing approaches. However, the formulation of bioinks is the foremost issue in 3D printing techniques. The printed scaffold comprises specific cells seeded on a biomaterial with a prespecified architecture to construct the functional tissues or organs, as illustrated in Figure 1. The 3D printing technology enables the construction of highly complex structures as scaffolds, with tunable

porosity, permeability, and mechanical properties, so that tissue models can be created.¹ 3D complex tissues are designed in Computer-Aided Design (CAD) by utilizing geometrical data obtained from medical imaging techniques, as X-ray imaging, magnetic resonance imaging (MRI), and micro-computerized tomography scan (μ -CT-scan).² Thus, 3D printing provides an opportunity for personalized patient-specific designs with extreme precision, low cost, and the creation of complex structures within a short time.

The printability of a bioink relies on various parameters, such as surface tension of the bioink, viscosity, printer nozzle type and the ability of crosslinking.³ The viscosity of the bioink should be adjustable for utilizing different devices. On the other hand, the bioink formulation should

promote cell attachment, proliferation and growth on the 3D construction. Functional groups are required for delivering various biochemical signals or biomolecules.⁴ The stiffness of the bioink affects cell survival.⁵ The bioink should demonstrate high resolution during printing. Besides, it has to be gelled *in situ*. A bioink should be mimicking the tissue structure with convenient mechanical behavior and

immunological compatibility.⁶ The predetermined structure of the tissue or organ structure should be printed with appropriate mechanical properties and should have functional groups on the material surface. After implantation, the product has to enable the transport of nutrients, oxygen, and metabolic waste. The above-mentioned parameters are the main properties of a bioink required for successful 3D printing.

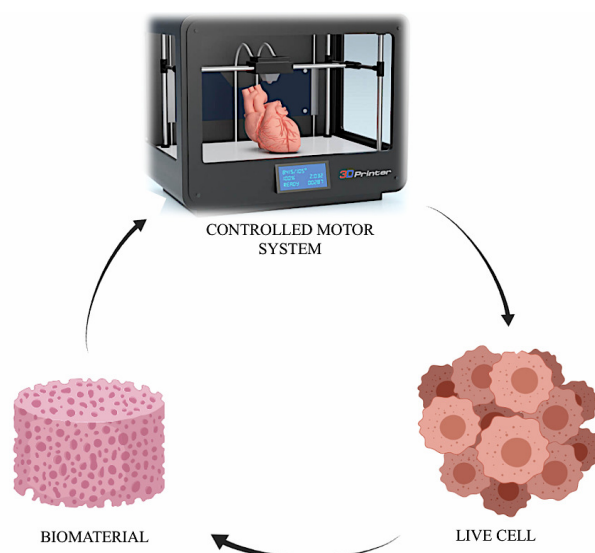


Figure 1: 3D printing of living tissues

There are a variety of biomaterials used as bioinks in 3D printing techniques, involving natural and synthetic polymers. Natural polymeric materials present some advantages, as biomimicking the composition of the extracellular matrix (ECM), biocompatibility and biodegradation. On the other hand, synthetic polymers ensure mechanical stability, photocrosslinking ability, temperature responses, *etc.* With growing environmental awareness, bio-based composite materials have drawn increasing attention all over the world. Thus, agarose,⁷ collagen,⁸ alginate,⁹ hyaluronic acid,¹⁰ and cellulose-based bioinks have been evaluated. Additionally, the great potential of these biohydrogels in forming 3D networks is similar to that of extracellular matrix (ECM), which makes them particularly attractive bioinks for printing applications.¹¹

Bacterial cellulose (BC) is widely used in tissue engineering and regenerative medicine applications in gel, membrane and powder forms. It is used either with its unique natural structure or in hydrolyzed and derivatized forms. Its chemical

structure is identical to that of plant-derived cellulose, but is free of hemicelluloses, pectin, and lignin. BC belongs to a promising class of biopolymers. It can be synthesized extracellularly by the gram-negative bacterial cultures of *Gluconacetobacter*, *Acetobacter*, *Agrobacterium*, *Achromobacter*, *Aerobacter*, *Sarcina*, *Azobacter*, *Rhizobium*, *Pseudomonas*, *Salmonella* and *Alcaligenes*. Among them, *Acetobacter xylinum* is the most common and effective producer of BC used for biomaterials.¹² In tissue engineering and regenerative medicine applications, BC has significant applications, involving blood vessels,¹³ bone,¹⁴ and urethral reconstruction.¹⁵ Although BC has the above-mentioned properties, for 3D printing a BC-based biomaterial, it is necessary to render the BC soluble, while maintaining its controllable and elastic properties. Moreover, the main superiority of BC as a biomaterial lies in its high nanofiber density (average distance between cellulose nanofiber and fiber area ratio). The mechanical behavior of scaffolds is highly affected by the BC nanofiber density. Besides, the nanofiber network

of BC directs cell behavior on it. Advantageously, if the nanofiber morphology of BC can be protected in the product obtained with printing, then we can manipulate the cell behavior on the material. BC, with a precise mechanical strength, is also a biocompatible material and mimics the native ECM due to its unique 3D nanofibrous network.

Considering that the actual obstacle to the use of BC is its inconvenient solubility in water and organic solvents, the present study aimed to obtain a soluble form of BC via a process used in the literature and to evaluate its suitability as a bioink in a 3D printing system. In this work, we have demonstrated the utility of the BC material in the 3D printing technology by printing a model vascular graft. This study demonstrated that BC is feasible for vascular graft printing, with a manageable morphology.

EXPERIMENTAL

Materials

Gluconacetobacter xylinus (ATCC® 10245TM) and commercial elastic resin were purchased from Formslab, ZnSO₄ was obtained from Sigma Aldrich (CAS No. 7446-20-0).

Production and solubility of bacterial cellulose and bioink preparation

The production of bacterial cellulose was performed by growing *Gluconacetobacter xylinus* (ATCC® 10245TM) in Hestrin–Schramm medium (5 g/L glucose, 5 g/L bactopectone, 2.5 g/L yeast extract) in 4 mM KH₂PO₄, 6 mM K₂HPO₄, adjusted to pH 5.0 by adding 1M HCl. The inoculum was performed by incubating *A. xylinum* at 30 °C, using a rotary shaker for 2 days. BC production was performed by inoculating the subculture at a proportion of 1:10 into Petri dishes statically. The formation BC nanofiber structure was observed in 7 days. BC was preserved after lyophilization. A 20% ZnSO₄ solution was prepared in deionized water. The dried BC was placed on a magnetic stirrer in the 20% ZnSO₄ solution for 2 days at 60 °C. Then, the dissolved BC solution–solvent solution was mixed with commercial resin at 1:10 wt% ratio.

3D Printing technique

Dissolved BC/zinc sulfate was mixed with commercial elastic resin at a 1:10 wt% ratio. The obtained bioink was evaluated for printing a human aorta vessel as a model designed in STL format. The bioink formulation of BC was printed by a Form2 printer, supplied from Formslab. The custom-designed Light Processing Unit (LPU) inside the printer uses a compact system of lenses and mirrors to deliver accurate and repeatable prints. The device works with

Low Power Stereolithography (SLA) technology, with XY resolution of 25 microns, that creates a layer thickness of 25-300 microns (0.001-0.012 inches). The equipment consists of a stainless-steel nozzle (21G orifice), high voltage power supply, a programmable syringe pump, X-Y stage motion control head, glass substrate holder and nozzle holder with Z-axis control. The distance between the nozzle and substrate was set to 1 mm for the experimental setup. The flow rate was kept at 100 μl h⁻¹ and the SLA parts were applied IPA rinsing and post-curing. The architecture was manipulated with 0 and 90 angle steps between two successive layers. Washing and curing steps were utilized to streamline and automate post-processing of the Form2 printer with an advanced heating system that precisely controls curing temperatures up to 80 °C.

The same 3D printing procedure was applied for printing a 3D vascular graft using only commercial resin as ink.

Characterization of BC

The morphology of BC and vascular graft was analyzed with scanning electron microscopy (Zeiss Evo LS10) (SEM). The BC membrane was lyophilized overnight at 65 °C before analysis. Au-Pd coating (Quorum SC-7620) was performed on samples for 1 min. Additionally, the BC membrane was magnified at 20.00 and 50.00 KX. Moreover, the vascular graft sample was also observed with a material microscope.

Thermal analysis

The thermal stability of the 3D printed aorta model was determined by the thermogravimetric (TG) and differential thermal analyses (DTA) by SII6000 Exstar TG/DTA 6300. Aluminum pans with 10-μg samples were placed under dynamic air. Nitrogen atmosphere at heating rates of 10 °C/min was applied. The mass loss was measured for 90 min in the range of 25 °C–1000 °C. The thermograms of each sample were analyzed.

Fourier transform infrared and RAMAN spectroscopy

The Universal ATR attachment and Perkin Elmer Raman Station 400F in the Perkin Elmer Spectrum™ 100 FTIR spectrometer were utilized for chemical characterization. The range of 4000–650 cm⁻¹, at a resolution of 4 cm⁻¹, and 32 accumulated scans were used. Raman spectra were excited using 785 nm radiation from a diode laser, where the laser power was 5 mW. Spectra were obtained over the range of 230–3500 cm⁻¹; 40 scans were utilized.

Surface area analysis

A Brunauer–Emmett–Teller (BET) surface area apparatus (Quantachrome, QuadraSorb SI) was used to determine the surface area of the 3D printed aorta. The sample of the aorta was placed in a degasser (quantochrome), then heated up to 75 °C for 18 h to

remove moisture. High purity nitrogen was used to measure the surface area by the absorption of nitrogen to the material surface for 189.3 min. P/P0 was analyzed in the range of 0.05–0.3.

Swelling and biodegradation analyses

The water holding capacity of the vascular graft was determined by the swelling test. The dry weight (W0) of the aorta sample was calculated. Then, the sample was cut as 2 cm² diameter pieces to immerse into the 10 mL of water at 37 °C. Every 24 hours, for three days, the weights of the aorta samples were calculated (Ws). The experiment was carried out in five replicates and the swelling ratio was calculated using the equation:

$$\text{Swelling ratio (\%)} = [(W0 - Ws)/W0] \times 100 \quad (1)$$

In vitro biodegradation of the 3D printed aorta was evaluated by the gravimetric method. A PBS solution containing lysozyme (1.5 µg/ml) was used. The 3D printed vascular graft sample was cut to 20-10 mm diameter and autoclaved at 120 °C for 20 min for sterilization. The vascular graft sample was immersed into the lysozyme enzyme at 37 °C for one month at 60 rpm in static condition. The 7th, 14th, 21st and 28th days were chosen for measuring the dry weights of the 3D printed sample and the lysozyme solution was refreshed. At the end of the measurement day, the tissue samples were soaked in water, and then dried with Whatman paper. After that, the tissue sample was lyophilized (Alpha 2–4 LD; Martin Christ Gefriertrocknungsanlagen, Osterode am Harz, Germany), and the mass loss was evaluated based on the following equation:

$$\text{Weight loss (\%)} = [(W0 - Ws)/W0] \times 100 \quad (2)$$

Protein adsorption capacity

BSA standard curves were utilized to determine the protein adsorption capacity of the 3D printed vascular graft sample. The standards were prepared at different concentrations as 1, 0.75, 0.5, 0.25, 0.062 mg/mL. For the determination, 3D printed vascular graft walls were chosen. The wall was cut at a size of 0.5 x 1 cm to insert within the Eppendorf tube and 500 µL of 1 mg/mL BSA solution was pipetted in a sample tube at 37 °C for 2 hours. To extract the non-adherent proteins, the samples were washed with distilled water at the end of the incubation time. The sample was placed into a new Eppendorf tube and incubated in 0.5% TritonX for 37 °C for 30 minutes to separate the proteins attached to the 3D printed aorta sample. Coomassie blue dye was utilized to calculate the protein adsorption of the 10 µl TritonX containing samples in a 24-well plate at absorbance 595 nm.

Dynamic mechanical analysis

A Perkin Elmer DMA 8000 analyzer was utilized to measure the dynamic mechanical behavior of the 3D printed vascular graft. The frequency of 1 Hz and a

heating rate of 5 °C/min from room temperature to 100 °C were applied. The 3D printed sample was prepared with the following dimensions: 17 mm in length, 7 mm in width, and a thickness of 0.03 mm.

In vitro studies

Seeding of HUVECs on 3D printed aorta

Prior to cell seeding, the 3D printed aorta was incubated in Endothelial Cell Growth media (ECG) for 1 hour. Filter paper was utilized to remove the media from the samples, after which they were placed in a 24-well plate. A cell suspension with a cell density of 3×10⁵ cell/cm² was seeded on each sample and incubated at 37 °C, 5% CO₂, 95% relative humidity for 4 h to allow optimal cell attachment. Then, 2 mL of ECG media was added to each 3D printed aorta and the well plate was placed back into the incubator. This was denoted as day 0. Media were changed every 2-3 days and samples were taken on hours 24, 52 and 72.

Cell viability, cell adhesion and expansion of HUVECs

Endothelial basal medium (Cell Applications, Inc.) was mixed with endothelial growth supplements (Cell Applications, Inc.) to obtain Endothelial Cell Growth media (ECG media). The human umbilical vein endothelial cells (HUVECs) (Cell Applications, Inc.) were thawed and transferred to a 75 cm² cell culture flask containing 15 mL of ECG media. The cell culture flask was incubated at 37 °C, with 5% CO₂, 95% relative humidity. The cells were passaged when they reached 80% confluence. Cells at passage number 5 were used for all the experiments. The MTT assay was utilized to determine the *in vitro* cytotoxicity and cell adhesion capacity of the 3D printed vascular graft on the HUVEC cell line. 10⁴ cells/well were seeded in a 96-well plate. The 3D printed vascular graft samples were cut into disc forms and placed in wells after being sterilized with 96% ethanol and subjected to UV radiation for 3 h. The medium was removed after overnight incubation and each well was treated with 100 µL of 3-(4-5-dimethylthiazol-2-yl)-2-5-diphenyltetrazolium bromide (MTT) (5 mg/mL in medium) incubated for 4 h. Then, the MTT solution was discarded and 100 µL of DMSO solution was added to each well to dissolve the formazan crystals. The optical density was determined at 570 nm by an Elisa reader (Thermo Scientific Multiskan Go, USA). The MTT analysis was performed in six replicates (n: 6). The results were presented as cell viability towards control (100% of survival). The adhesion and proliferation capacity of the 3D printed aorta was determined for 24, 52 and 72 hours at 37 °C, under 5% CO₂ atmosphere.

Fluorescence microscopy and histochemistry analysis

The vascular graft samples were washed in PBS twice to remove residues, then covered with 3.7% formaldehyde (Sigma-Aldrich) and left for 2 h at room

temperature. Samples were immersed in PBS and kept till analysis. 0.1% Triton X100 (Sigma-Aldrich) was added to cover the samples and left for 45 min at +4 °C. The solution was discarded, the samples were washed twice in PBS. DAPI staining solution in PBS (5 $\mu\text{m}/\text{mL}$) was added to cover the samples for 30 min. The DAPI was used to stain cell nuclei. Rhodamine phalloidin was used to visualize the actin filaments. The samples were rinsed in PBS and stored in PBS until visualization. For analysis, a phase-contrast microscope (Leica Digital Microscopes Inverted) was used.

The vascular graft specimen was collected and fixed in 4% neutral buffered formalin for 24 h to utilize for histochemical staining. Afterward, explants were dehydrated in a series of graded alcohol and embedded in paraffin blocks, sectioned at 6 μm thickness and stained with hematoxylin and eosin (H&E). Images were obtained by a fluorescent microscope (LEICA DMi8, Leica Microsystems GmbH, Germany).

Rheological characterization of BC-based bioink to control printability

The rheological behavior of the BC-based bioink was characterized using a digital rheometer (MARSIII, Thermo Scientific, Newington, NH, USA), fitted with a parallel plate (35 mm radius), to investigate shear thinning properties. For rheological characterization, the BC-based bioink was vortexed vigorously and degassed in a centrifuge at 168 \times G for 2 minutes. The experiment was performed under 0.1 to 1000 Pa at a frequency of 1 Hz and a temperature of 25 °C. Step-stress measurements were performed at high-magnitude (300 Pa) and low-magnitude (0.5 Pa) stress.

Statistical analysis

Statistical comparisons were performed using t-test analysis. P-values <0.01 were considered statistically significant.

RESULTS AND DISCUSSION

Production and solubility of BC and bioink preparation

The polymerization of BC occurs into single, linear β -1,4-glucan chains. BC is secreted outside the cells from pores located on the membrane. The first structure of the bacterial cellulose is formed as sub-fibrils consisting of 10–15 nascent β -1,4-glucan chains aligned in parallel form, interspersed among amorphous regions, representing 90% of the total volume of the material. Then, a microfibril structure is obtained and, finally, the loosely wound ribbon structure of microfibril bundles is created, including approximately 1000 individual glucan chains.

The dried BC was placed on a magnetic stirrer for 2 days at 1:10 wt% at a temperature of 60 °C. Then, the BC was sonicated using a sonifier (Branson Sonifier 250, BRANSON) at a power output of 100% for 1 h. After that, the BC samples were centrifuged at 6000 rpm for 600 s. After each centrifugation step, the supernatant was removed and fragmented BC was obtained. The BC was blended with 20 wt% commercial resin in a 5:95 wt ratio and the final blend was magnetically stirred for 1 h at 23 °C, as shown in Figure 2.

3D Printing technique using BC-based bioink

The 3D geometry of the vascular graft was modeled in STL format. The hole pattern of the aorta was designed and converted into the desired format, as shown in Figure 3. The software converted the imported STL file into print paths by slicing them into layers and ensuring contour and fill-paths for each layer based on specific print parameters. Before 3D printing, the composite bioink containing BC/zinc sulphate and resin was mixed to form an injectable homogeneous paste at 37 °C. The obtained BC-based bioink was printed along the X-Y target paths for each layer, and after each layer was completed, the print stage was translated Z.

The high-powered laser is guided by custom galvanometers, creating each layer with exceptional detail. A sliding peel mechanism gently removes the part from the print bed, while a wiper glides across the optical window. A responsive heating system warms the bioink to a constant temperature (80 °C). The standard printing parameters used in our experiment were: 25 mm path width, 30 mm path height. The thickness was 1 cm.

Characterization of BC

The 3D nano-network structure of the 3D printed vascular graft sample was observed by SEM and a material microscope. The lyophilized form of BC and of the vascular graft was coated with gold for 75 seconds and the surface morphology of the samples was examined using SEM. As seen in Figure 4, the BC has an extensively porous surface due to its high crystallinity. Particularly, after printing, the SEM images also revealed that the micropore size, porosity and nanofiber diameter can be kept relatively constant.

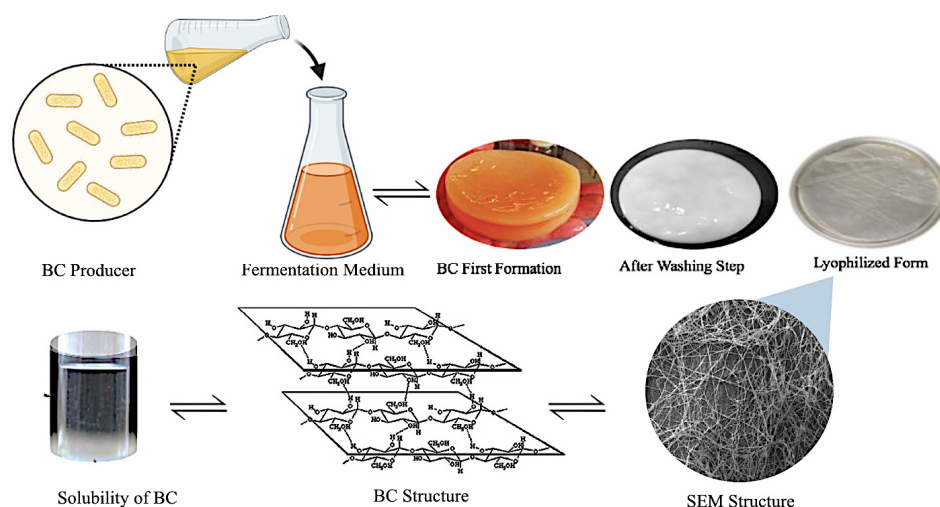


Figure 2: Production and dissolved form of BC

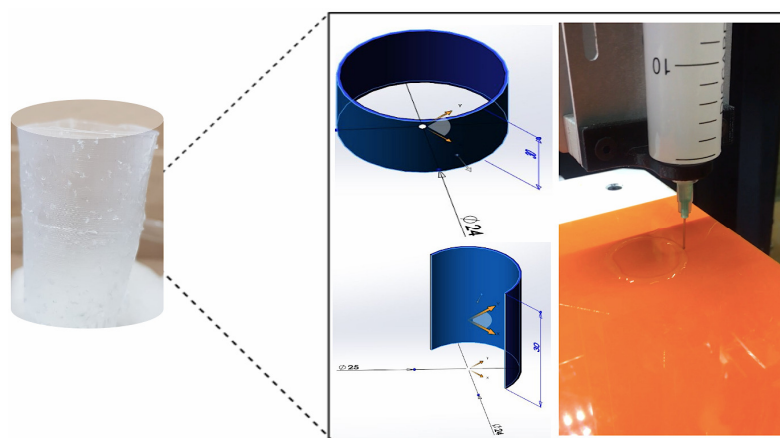


Figure 3: 3D printed model with BC-based bioink

Thermogravimetric analysis

In thermal gravimetric analysis (TGA), the mass of the sample is calculated over time based on the temperature changes. The thermal degradation behavior of the aorta was examined by thermogravimetric analysis and the results are provided in Figure 5. The mass loss of the sample was calculated at the first point of the TGA curve as 1.75%. The 1.75% weight loss at the beginning of the TGA curve is due to evaporation of surface water and dehydration of the material. At 361 °C, the mass loss was 22.72% and at 421 °C the mass loss was 52.4%. Throughout 800 °C, the mass losses were slower and moderate.

Chemical characterization of samples

Fourier transform infrared spectroscopy (FT-IR) was used to analyze the interaction of

chemical groups between the components of BC/zinc sulphate and resin in the 3D printed aorta. The FTIR spectrum presents the characteristic peaks of the resin and BC. The soluble form of BC exhibited a characteristic FTIR band around 1740 cm^{-1} and peak intensity increases with raising the degree of oxidation. The following peaks were observed: H_2O at 3411 cm^{-1} ,¹⁶ aliphatic C-H bending at 2921 cm^{-1} ,¹⁷ C=O stretching band at 1721 cm^{-1} , CH_3 asymmetric bend binding at 1235 cm^{-1} , C-O-C bond strain at 1375 cm^{-1} , indicating the bending, as summarized Table 1.¹⁸ FTIR spectroscopy results were confirmed by Raman spectroscopy (Fig. 6 a and b). The Raman spectroscopy revealed that deformations and stresses in the bond structures occurred as a result of blending the dissolved BC with the resin.

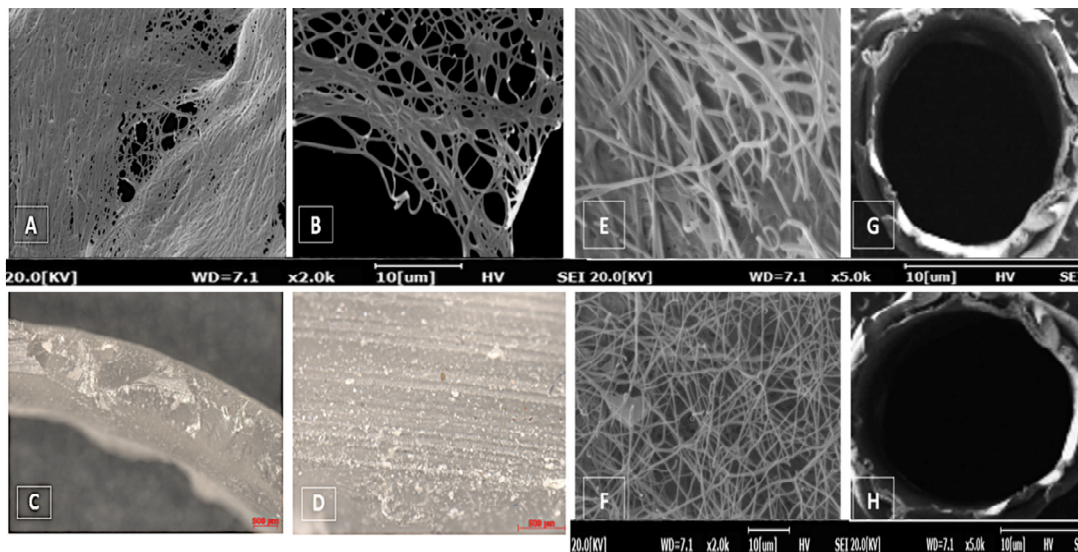


Figure 4: SEM microphotographs of 3D nano-network structure of BC (A and B); Material microscope images of 3D printed aorta structure (C and D); and SEM microphotographs of 3D nano-network structure of 3D printed aorta (E and F) and cross-section of 3D printed aorta (G and H)

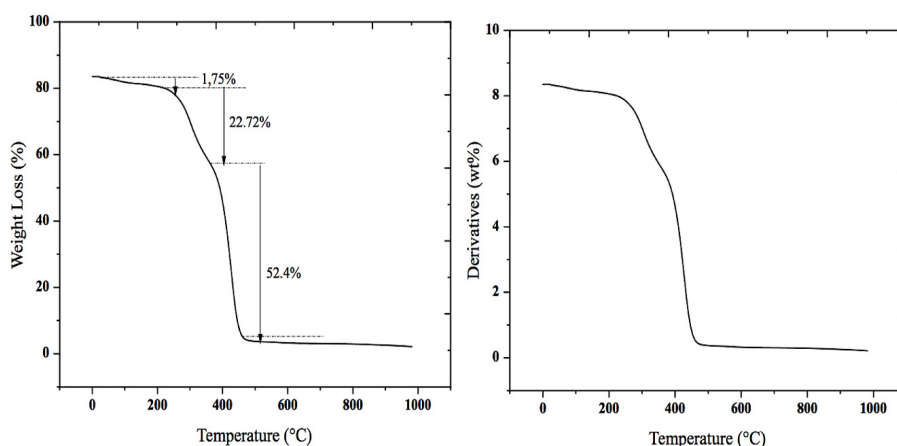


Figure 5: TG/DTA analysis of 3D printed aorta

Surface area of 3D printed sample

The surface area of the 3D printed sample was measured as 8.290 m²/g, as summarized in Table 2, depending on the results of the Brunauer-Emmett-Teller (BET) analysis, with a 0.097 correlation coefficient. In this study, we aimed to provide a structure mimicking the natural ECM's surface area and mechanical strength.

Swelling and biodegradation analyses

The 3D printed aorta was rinsed in water to determine the water retention capacity (WRC). The results are shown in Figure 7. For the analysis, five replicates of the tissue samples were immersed in water and their mass changes were

determined after 1, 24 and 48 hours. The swelling analysis showed that the WRC of the 3D printed sample increased by 5% at the end of 24 hours (standard error ± 0.18). Additionally, at the end of 48 hours, the WRC increased by 9% (standard error ± 3.34). The mass loss of the 3D printed vascular graft samples was determined after immersion into PBS solution (1.5 $\mu\text{g}/\text{mL}$) with lysozyme enzyme for 28 days. The results were given in Figure 7. No mass loss of the 3D printed aorta sample was determined. In this study, the developed commercial resin-BC composite is considered to be well appropriate for tissue structure formation based on the biodegradation studies.

Table 1
Assignments of FTIR spectra

Peaks (cm ⁻¹)	Assignments
3411	H ₂ O
2921	Aliphatic C-H stretching band
1721	C=O stretching band
1375	C-O-C stretching band
1235	CH ₃ asymmetric bending band

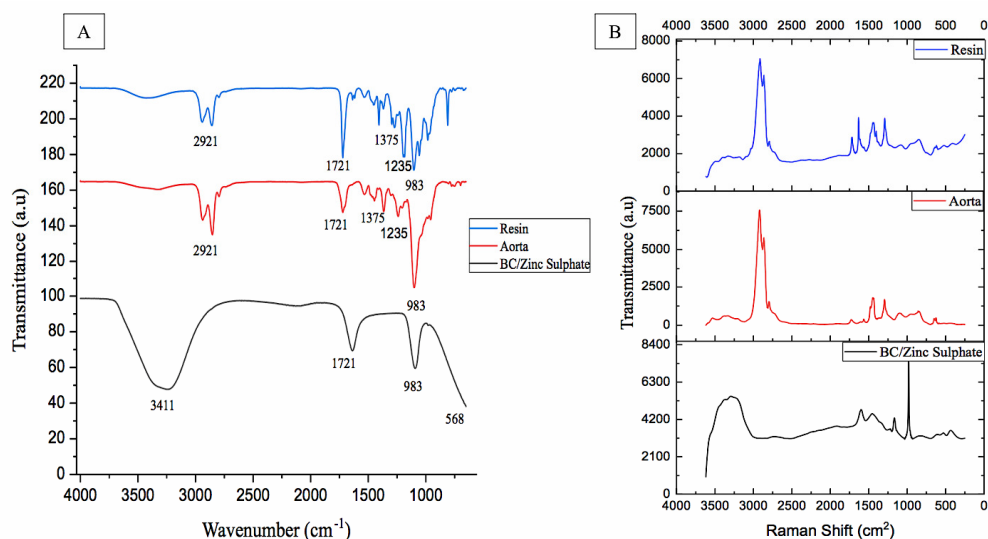


Figure 6: a) FT-IR spectra of 3D printed aorta, resin and BC/zinc-sulphate; b) Raman spectra of 3D printed aorta, resin and BC/zinc-sulphate

Table 2
BET summary of 3D printed aorta

BET summary	
Slope	16.570
Intercept	4.053e+02
Correlation coefficient	0.097
C constant	1.041
Surface area	8.29 m ² /g

Protein adsorption capacity

The standard curve of different BSA standard concentrations (1, 0.5, 0.25, 0.125 and 0.625 mg/mL) was chosen to calculate the protein adsorption capacity of the 3D printed vascular graft walls. In the study, the BSA standard protein adsorption was calculated as 0.99 mg/mL (standard error ± 0.03). The BSA standard was utilized as the control group, with a ratio of 100%. In this perspective, the protein adsorption capacity of the 3D printed aorta walls was calculated as 7% (standard error ± 0.02) (Fig. 8). The hydrophilic or hydrophobic character of the

surface of a biomaterial determines the efficacy of protein adsorption and cell attachment on the surface. Specifically, the surface properties of the biomaterial determine the amount, type, and conformation of the proteins adsorbed to the surface, and affects cell binding and cell proliferation to the membrane. The free surface energy is the sum of the polar and non-polar components of the material surface. Besides, the hydrophilicity degree of a biomaterial surface helps us to foresee the possible degree of cell adhesion and proliferation on a biomaterial.¹⁹

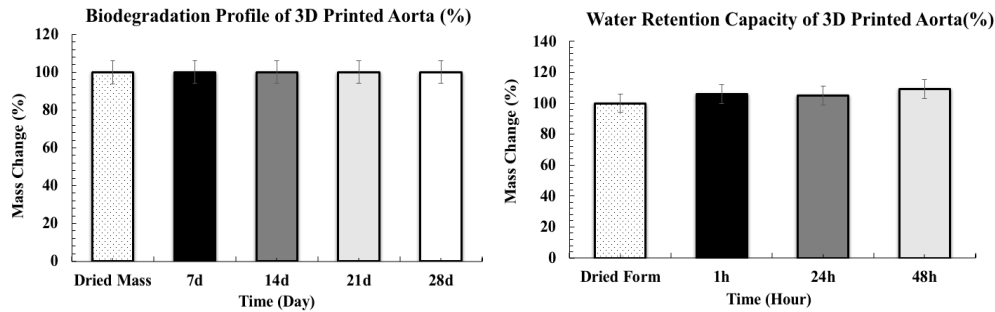


Figure 7: Mass changes of 3D printed aorta sample

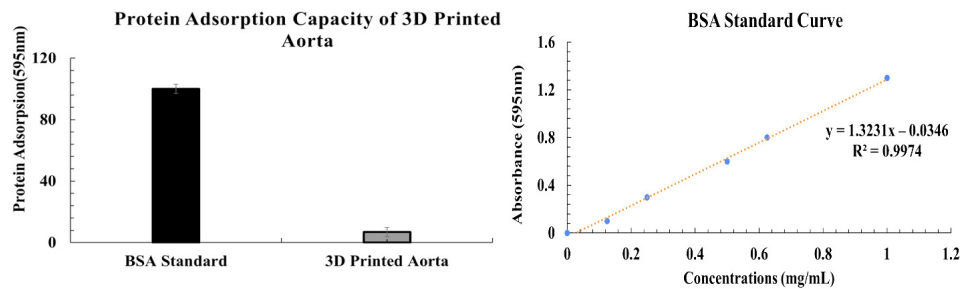


Figure 8: Protein adsorption capacity of 3D printed aorta

Table 3
Mechanical properties of 3D printed aorta

3D printed aorta	Elongation at break	Young's modulus
	ϵ_k (%)	E (N/mm ²)
	87.591±3.01	172.083±10.564

Dynamic mechanical analysis

In the study, the mechanical strength of the 3D printed aorta sample was measured and the results are given in Table 3. The elasticity modulus of the sample was 172.083 (standard error ± 10.56) (N/mm²). The elongation at break of the sample was determined as 87.591% (standard error ± 3.01). The modulus of elasticity provides information about the deformations occurring under stress. It is related to the ability of a specimen to resist changes of shape without cracking. The combination of high ultimate tensile strength and high elongation leads to materials of high toughness.²⁰

In vitro cytotoxicity, cell adhesion and expansion of HUVECs

Cell adhesion and cytotoxicity are critical points for the biocompatibility of 3D printed materials. The ideal tissue construction should support cell adhesion, proliferation and differentiation. The cytotoxicity effect and cell adhesion capacity of the 3D vascular graft was

evaluated. The mitochondrial activity test (MTT) has been utilized on human umbilical vein endothelial cells (HUVECs), as shown in Figure 9. The results of cell viability were expressed as the percentage of control groups (negative control: only medium, positive control: phenol). The cell viability on the resin 3D printed vascular graft was compared with that on the BC-resin composite containing 3D printed vascular graft.

It is a well-known fact that BC is a highly biocompatible material used in tissue engineering and regenerative medicine. Therefore, we supposed that the BC additive will increase cell viability and attachment. The cell viability observed on the only resin-containing 3D printed aorta was 75.84% (standard error ± 3.53), while on the BC-resin 3D printed aorta, it was found to be 100% (standard error ± 4.53). The cell viability of the negative control was 100% (standard error ± 0.3). Thus, the 3D aorta printed with BC/resin bioink increased the viability of the cells based on the MTT analysis. It exhibited cell viability by 44% higher than that of the only resin-based 3D

printed vascular graft and therefore, it can be considered a non-toxic and cyto-compatible material, based on ISO 10993:5 standard regulations.²¹ According to these results, the BC-resin composite printed structure of aorta can be regarded as biocompatible.

On the other hand, HUVECs were seeded as 10^5 cells/1 cm on the 3D printed vascular grafts in 96-well plates to determine the cell adhesion and proliferation rates. Samples were incubated at 37 °C in 5% CO₂ atmosphere for 2 hours for first attachment of the cells. The morphology of the HUVEC line was observed after 24, 52 and 72 hours. The rate of the cell line adhesion was compared with the control groups (negative control: only medium, positive control: phenol). It has been observed that the number of HUVECs considerably increased day after day. However, according to the MTT results, while cell adhesion

on the BC-resin 3D printed aorta was determined as 89.02% (standard error ± 1.3) after 24 h, 92.01% (standard error ± 2.4) after 52 h, 100% after 74 h, which indicated the rapid proliferation of HUVECs grown on the reached 55.02% (standard error ± 1.3) after 24 h, 56% (standard error ± 2.1) after 48 h and 58.04% (standard error ± 1.8) after 72 h, as shown in Figure 9.

Fluorescence microscopy and histochemistry

At the end of the 72 h, cell attachment was examined by immunofluorescence staining, along with DNA quantification. Normal fibroblastic morphology was observed for the HUVEC cell lines. The cell adhesion capacity at the end of the 72 hours to the vascular graft sample was confirmed by immunofluorescence staining by DAPI. The DAPI stains the cell nuclei.

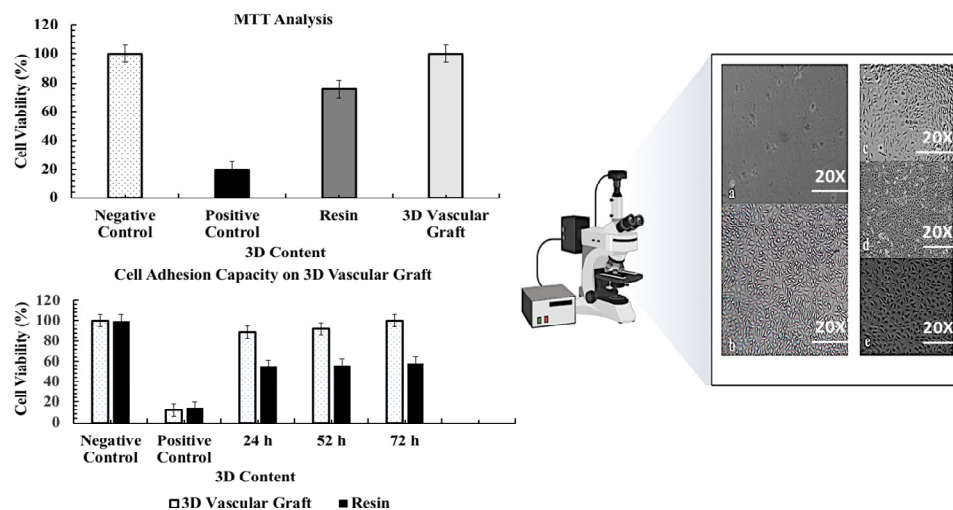


Figure 9: Cytotoxicity and cell adhesion of 3D printed aorta (MTT); a – positive control, b – negative control, c – 24 h cell attachment, d – 52 h cell attachment, e –72 h cell attachment

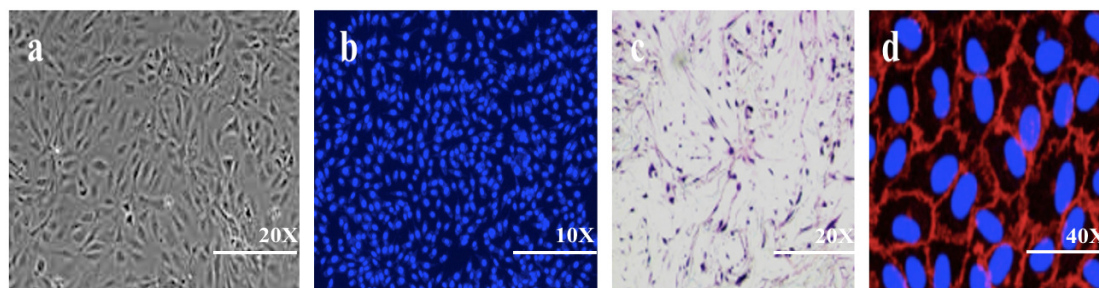


Figure 10: Cell attachment after 72 hours examined by a) inverted microscopy, b) DAPI staining, c) Rhodamine phalloidin and DAPI, and d) H&E staining

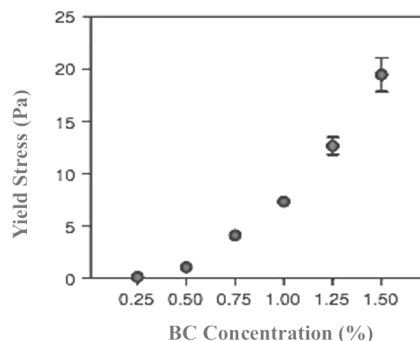


Figure 11: Change of yield stress according to BC content

On the other hand, we did not observe any significant protein adsorption. Protein adsorption on the vessel surface narrows the vessel lumen and stimulates cell proliferation, causing neointimal hyperplasia, which is never a desirable issue. After 72 h, we confirmed both cell nuclei and protein construction with H&E histologic staining, as shown in Figure 10. Additionally, for the actin filament construction, Rhodamine phalloidin was utilized during DAPI staining on nuclei of HUVEC cell lines on the 3D printed aorta sample.

Rheological characterization of BC-based bioink

The physical stability of the printed hydrogel structures was affected significantly by the rheological properties of the inks. As the BC content increased, the viscosity of the ink rose as well, because of higher crosslinking with the BC. However, viscosity was lowered by the shear force acting at the wall surface of the needle, allowing the BC-based bioink to discharge easily from the needle. The yield stress of the BC-based bioink increased with the BC content, as shown in Figure 11.

Discussion

The natural biopolymer bacterial cellulose is an organized fibril structure at the nanoscale. However, BC nanofibers have been distributed randomly. The hydroxyl groups of BC tend to form hydrogen bonds with neighboring chains to stabilize its structure in a crystalline pattern. The crystallinity relies on the versatility of possible intra- and intermolecular bond associations. The crystalline structure of BC affects its solubility. The dissolution of BC mainly undergoes a swelling stage, followed by a dissolving stage. The translucent gel film of BC has a thickness of

1-1.5 cm in the wet state and 20-40 μm in the dry state, as reported in the literature, thus it undergoes high volume transformation, over 300 times, from a dry state to wet state.²² The dissolution process was affected by the volume transformation. Therefore, the form of BC used in the present study (lyophilized) had great influence on solubility. The results showed that the water content strongly influences the dissolved BC in zinc-sulfate aqueous solutions (20% of ZnSO_4). Temperature is an auxiliary element for breaking hydrogen bonds in the BC membrane, contributing to its dissolution in an inorganic solvent, as seen in our study. Additionally, the Lewis acidity of Zn^{+2} further utilizes a weak hydrogen bond acceptor. Neither molecular ion demonstrates a dipole. This structural description of a strong hydrogen-bond donation would seem ideally suitable for dissolving BC with extensive intra- and intermolecular hydrogen bonding.

If the BC morphology can be preserved at the nanoscale, its tensile strength and toughness are increased, so it can be further used in tissue engineering and regenerative medicine studies, especially in 3D tissue and organ construction. Also, it is necessary to know the optimum strength values of the printed aorta to be beneficial *in vivo*. Thus, it is important to determine the mechanical properties of biomaterials used in printing technology in order to predict their suitability for the target application. Native soft tissues or organs have a Young's modulus ranging from 0.1 to 1000 kPa.²³ The Young's modulus of native pulmonary artery is 0.040 MPa. Also, tissue stiffness was determined at two different stress levels, 72.8 kPa and 120 kPa, corresponding to the physiological stress of aorta.²⁴ In this study, the mechanical behavior of vascular grafts was optimized. As reported in the literature, micro/nanofibers

matching the native tissues' mechanical properties have been commonly used as fillers.²⁵ BC consists of a hierarchical fibril structure, originating from the strong intramolecular and intermolecular hydrogen bonding that provides high tensile strength and elastic modulus.²⁶ The exceptional mechanical properties of BC-based vascular grafts are provided by micro/nanofibers morphology with a large surface to volume ratio, high surface area.²⁷ In the literature, BC/gelatin has been used for 3D printing and the results showed the Young's modulus of BC/gelatin scaffold reached 1.84 ± 0.13 MPa, about 12 times higher than that of the pure gelatin scaffold (0.15 ± 0.04 MPa).²⁸ The Young's modulus of a nanocellulose-alginate hydrogel scaffold has been also described, with stiffness in the range from 70 to 250 kPa at 30% strain.²⁹ Ultimately, BC has a great fiber length/fiber diameter ratio over 50 and high crystallinity (>80%), compared to other cellulosic materials, and these properties provide suitable mechanical behavior to BC. In the present study, the elasticity modulus (172.083 ± 10.564 N/mm²) values demonstrated to be appropriate for tissue construction.³⁰ As expected, the presence of BC in the printing bioinks for printing grafts played a critical role in promoting mechanical properties.

Herein, we demonstrated that *in situ* fabrication of BC combined with commercial resin generates a great biocompatible construction, with highly organized nano morphology. The nano characteristic provides high water retention capacity and ideal model ECM structure to the 3D vascular graft. The characterization analysis showed that BC-based bioinks exhibited good shape, maintaining the ability for printing soft tissue models. The size of the bacterial cellulose fibrils ranged between 60 and 100 nm. The nanofibers with a width of about 100 nm provide the 3D environment for hydrogel scaffolds due to almost similar construction with collagen fibrils of ECM.³¹ The surface properties of a biomaterial, such as surface roughness, hydrophilicity, and surface energy, are critical for cell attachment, proliferation, and differentiation. Surface roughness affects the cellular response and is critical for cell fate.³² It is known that the scaffold pore structure and integrity have considerably affected cell alignment, proliferation, and viability *in vitro*.³³ When the dense struts of scaffolds were compared with the smooth surface, scaffolds having struts with a porous surface structure exhibited suitable property for tissue regeneration.³⁴ Therefore, the

BC/zinc sulfate-resin composite has high interfacial adhesion and interactions due to the hydrogen bonds. Moreover, after printing, the porous nanofibrous structure of the vascular graft is similar to the structure of native ECM. Although in the literature, the 3D system has been described as lacking porous structure, which cannot fully mimic the natural porous nanofibrous ECM, this result provides us a robust method to control nanofiber density inside a porous 3D scaffold.³⁵ The pore size of BC is one of its critical characteristics, which has been described as having a significant influence on the swelling ability of BC.³⁶ Karol *et al.* also discussed about the swelling ability of BC.³⁷ In tissue engineering and regenerative medicine, the swelling behavior has a considerable effect on cell adhesion, proliferation, and differentiation.³⁸ In this study, the developed BC-resin bioink showed good porosity and fibril morphology, which increased the swelling property of the 3D printed vascular graft. Furthermore, the printed geometry showed a hierarchical porous structure, which could induce cellular infiltration, as well as new tissue ingrowth, as shown in tissue engineering and regeneration studies.²⁷

At the same time, the biodegradation analysis of the vascular graft is another crucial factor. The vascular grafts have to present resistance to biodegradation under *in vivo* conditions. The blood is made up of plasma, which contains water, salts, and protein, and the solid part of blood contains red blood cells, white blood cells, and platelets. Thus, vessels in our body contact many components of the biological microenvironment. The vascular construction of a 3D printed material should remain stable and not affected by body fluids, particularly by blood. Therefore, during the 28-day biodegradation analysis, lysozyme was utilized and the results (Fig. 7) showed that the 3D printed vascular graft exhibited suitable construction in for resisting biodegradation.

Moreover, in this study, FTIR and RAMAN analyses were utilized to understand the chemical construction of the vascular graft. The spectrum demonstrates the typical curves when BC is dissolved in zinc sulfate. The FT-IR band of BC/zinc-sulfate showed that no chemical reaction had happened during the coagulation and dissolution of BC.³² There were physical cross-links between BC and zinc sulfate, which resulted from the combination of hydrogen bonds and electrostatic interactions or hydrogen bridges.³⁹

Also, a large number of hydrogen bonds existed between resin and BC/zinc sulfate. In the literature, Deniz *et al.* described a BC based composite bioink formulation used in bone tissue engineering with similar FTIR results.¹⁶ Moreover, Esra *et al.* reported similar results for a BC and PCL composite bioink formulation.¹⁸

The surface area was analyzed by BET to verify the SEM results, which are critical for more information about the morphology of the 3D printed vascular graft. The surface area of 3D-printed vascular grafts vary depending on their porosity.⁴⁰ Increases in the number and size of the pores result in the extension of the surface area.⁴¹ In the present study, the surface area of the 3D printed vascular graft was determined as 8.290 m²/g, which is also a suitable result, as illustrated in the literature.⁴²

The multiple degradation steps indicate that the intermediate degradation products are stable over certain temperature ranges based on the TG curve. The BC-based bioink is resistant to the autoclaving temperature of 121 °C. The hydrogen bond-linked water molecules can be lost in the first stage as 1.75%, based on the TGA curve. The second mass loss is observed between 200 to 400 °C (361 °C), which is assigned to thermal decomposition of cellulose.⁴³ The thermal degradation behavior is affected by some structural parameters, as molecular weight, crystallinity, and orientation of the fibers.⁴⁴ In the literature, similar results have been reported for BC.⁴⁵

The prediction and control of the complex interactions between biomaterials and adsorbed proteins have not yet been elucidated in detail. Foreign body reaction occurring around implants and thrombosis on surfaces within contact with body fluid (blood) are the major reactions encountered in the case of implants. In particular, for vascular graft, protein adsorption poses risks for thrombosis within the body. The adsorption of proteins to the walls of the 3D printed aorta causes thrombosis. One of the most widespread birth defects worldwide is congenital heart disease (CHD). Specific defects exist in different patients due to anatomical differences, which affect the treatment of CHD. Therefore, appropriate design and adaptation of grafts should be ensured for a beneficial CHD treatment. However, the grafts currently used suffer from an increased risk of thromboembolic complications. Thus, in this study, the absence of protein adsorption to the vascular graft revealed that

elimination of the thrombosis risk is possible, due to the inner wall structure of the vascular graft containing BC. In the literature, poly(ethylene glycol) and its derivatives are considered as the most protein-repelling compounds in biomaterials. On the other hand, low and intermediate concentration levels of PEG-based biomaterials sensitively regulate cell adhesion processes.

The biocompatibility of the composite scaffolds was assessed in terms of cell proliferation and morphology. After 24 h of culture, cells began to spread and elongate along the direction of the microfibers of the vascular graft. After 48 h, the proliferated cells not only covered the entire surface of the 3D printed vascular graft, but also infiltrated through the pores between fibers. At the end of the 72 h, the cultured cells proliferated and started to form clusters on the vascular graft composite scaffold sample. According to the study by Fernanda *et al.*, the BC surface influences cell behavior (adhesion, proliferation, secondary necrosis) through the cell-nanofibers interaction.⁴⁶ The attachment capacity of the 3D printed aorta revealed that the BC-resin composite construction increased cell adhesion. At the end of the 72 hours, the 3D vascular graft sample was confirmed as an ideal construction by inverted microscopy, DAPI, H&E staining and Rhodamine phalloidin staining. In the literature, similar results have been reported.²⁸ The observed high level of cell adhesion and viability confirms that the 3D printing method using BC-based bioink was not detrimental to cell health and it can enhance the viability of cells on scaffolds.

CONCLUSION

In tissue engineering strategies, cells are seeded on synthetic, natural, or composite scaffolds. However, traditional scaffold fabrication techniques remain incapable of developing porous 3D support materials with the desired architecture. With all considerations, we can conclude that 3D printed scaffolds fill the most critical lack in tissue engineering.

The present study aimed to optimize a novel bioink formulation and its 3D printing parameters. The bioink formulation is the foremost issue in 3D printing strategies for creating appropriate tissue or organ construction. Bacterial cellulose is a well-known hydrogel and has an insoluble structure as all hydrogels. However, due to its unique natural biocompatibility, it is a widely

used biomaterial. However, since BC is produced by bacteria, it can only be obtained as a sphere or a film. The bioink developed in the study was bacterial cellulose-based, however, the problem of the insolubility of BC was the biggest challenge. This study presents the development and application of fully 3D-printed fabrication of non-cellular BC and resin composite scaffolds for vascular tissue engineering. To the authors' knowledge, it is the first report in the literature where the solubility of BC was optimized with zinc sulfate and the composite was made with resin. The printed vascular grafts present complex structures, with customized macroscale geometry as a vessel, with controlled microscale architecture in terms of porosity and surface roughness. The composite with BC and resin was used to improve the shape fidelity and the mechanical properties of the 3D printed scaffolds. The algorithms were developed in a computer-aided system with STL format. The BC and resin composite exhibited enhanced biocompatibility and facilitated cellular proliferation. It will be used in a further study for supporting the growth of target tissues, to endorse its use for tissue engineering applications.

The two critical parameters for vascular grafts are mechanical strength and thrombosis. We obtained a graft with proper mechanical strength. Besides, protein adhesion to the vessel, which can cause thrombosis over time, was not observed. The *in vitro* evaluation showed that the composite 3D printed vascular graft had excellent biocompatibility and cell adhesion ability, according to the MTT analysis. In conclusion, the BC-based bioink formulation developed in the present study has a great potential for vascular tissue engineering applications. 3D printing can be used for low-cost BC-based small diameter graft production.

REFERENCES

- ¹ S. V. Murphy and A. Atala, *Nature Biotechnol.*, **32**, 773 (2014), <https://doi.org/10.1038/nbt.2958>
- ² B. Guillotin, A. Souquet, S. Catros, M. Duocastella, B. Pippenger *et al.*, *Biomaterials*, **31**, 7250 (2010), <https://doi.org/10.1016/j.biomaterials.2010.05.055>
- ³ A. Tirella, A. Orsini, G. Vozzi and A. Ahluwalia, *Biofabrication*, **1**, 045002 (2009), <https://doi.org/10.1088/1758-5082/1/4/045002>
- ⁴ C. Chen, S. Bang and Y. Cho, *Biomater. Res.*, **20**, 10 (2016), <https://doi.org/10.1186/s40824-016-0057-3>
- ⁵ A. Tirella, F. Vozzi, C. De Maria, G. Vozzi, T. Sandri *et al.*, *J. Biosci. Bioeng.*, **112**, 79 (2011), <https://doi.org/10.1016/j.jbiosc.2011.03.019>
- ⁶ M. Hospodiuk, M. Dey, D. Sosnoski and I. T. Ozbolat, *Biotechnol. Adv.*, **35**, 217 (2017), <https://doi.org/10.1016/j.biotechadv.2016.12.006>
- ⁷ Q. Gu, E. Tomaskovic-Crook, R. Lozano, Y. Chen, R. M. Kapsa *et al.*, *Adv. Healthc. Mater.*, **5**, 1429 (2016), <https://doi.org/10.1002/adhm.201600095>
- ⁸ X. Yang, Z. Lu, H. Wu, W. Li, L. Zheng *et al.*, *Mater. Sci. Eng. C*, **83**, 195 (2018), <https://doi.org/10.1016/j.msec.2017.09.002>
- ⁹ Y. Zhang, Y. Yu, H. Chen and I. T. Ozbolat, *Biofabrication*, **5**, 025004 (2013), <https://doi.org/10.1088/1758-5082/5/2/025004>
- ¹⁰ L. Ouyang, C. B. Highley, C. B. Rodell, W. Sun and J. A. Burdick, *ACS Biomater. Sci. Eng.*, **2**, 1743 (2016), <https://doi.org/10.1021/acsbiomaterials.6b00158>
- ¹¹ M. Schaffner, P. A. Rühls, F. Coulter, S. Kilcher and A. R. Studart, *Sci. Adv.*, **3** (2017), <https://doi.org/10.1126/sciadv.aao6804>
- ¹² P. R. Chawla, I. B. Bajaj, S. A. Survasve and R. S. Singhal, *Food Technol. Biotechnol.*, **47**, 107 (2009), <https://hrcak.srce.hr/file/59853>
- ¹³ A. Bodin, L. Ahrenstedt, H. Fink, H. Brumer, B. Risberg *et al.*, *Biomacromolecules*, **8**, 3697 (2007), <https://doi.org/10.1021/bm070343q>
- ¹⁴ S. Park, J. Park, I. Jo, S.-P. Cho, D. Sung *et al.*, *Biomaterials*, **58**, 93 (2015), <https://doi.org/10.1016/j.biomaterials.2015.04.027>
- ¹⁵ X. G. Lv, C. Feng, Y. Liu, X. Peng, S. Chen *et al.*, *Theranostics*, **8**, 3153 (2018), <https://doi.org/10.7150/thno.22080>
- ¹⁶ D. Aki, S. Ulag, S. Unal, M. Sengor, N. Ekren *et al.*, *Mater. Des.*, **196**, 109094 (2020), <https://doi.org/10.1016/j.matdes.2020.109094>
- ¹⁷ R. Auta, G. Adamus, M. Kwiecien, I. Radecka and P. Hooley, *African J. Biotechnol.*, **16**, 470 (2017), <https://doi.org/10.5897/AJB2016.15486>
- ¹⁸ E. Altun, N. Ekren, S. E. Kuruca and O. Gunduz, *Mater. Lett.*, **234**, 163 (2019), <https://doi.org/10.1016/j.matlet.2018.09.085>
- ¹⁹ M. A. Yıldırım, M. Demirbilek and N. Türkoğlu, *Mater. Technol.*, **36**, 1 (2020), <https://doi.org/10.1080/10667857.2020.1734722>
- ²⁰ <https://omnexus.specialchem.com/polymer-properties/properties/elongation-at-break#A-C>
<https://omnexus.specialchem.com/polymer-properties>
- ²¹ International Standards Organization, Biological Evaluation of Medical Devices, ISO 10993-5:2009 Biological evaluation of medical devices - Part 5: Tests for *in vitro* cytotoxicity (2009)
- ²² J. Shiru, O. Hongyu, M. Xia, L. Li and Z. Kairui, *J. Cellul. Sci. Technol.*, **10**, 25 (2002)
- ²³ I. Levental, P. C. Georges and P. A. Janmey, *Soft Matter*, **3**, 299 (2007), <https://doi.org/10.1039/B610522J>
- ²⁴ A. N. Azadani, S. Chitsaz, P. B. Matthews, N. Jaussaud, J. Leung *et al.*, *Ann. Thorac. Surg.*, **93**, 87 (2012), <https://doi.org/10.1016/j.athoracsur.2011.08.002>

- ²⁵ W. Song, D. Liu, N. Prempeh and R. Song, *Biomacromolecules*, **18**, 3273 (2017), <https://doi.org/10.1021/acs.biomac.7b00927>
- ²⁶ P. Wei, J. Cai and L. Zhang, *Chinese J. Chem.*, **38**, 761 (2020)
- ²⁷ L. Huang, X. Du, S. Fan, G. Yang, H. Shao *et al.*, *Carbohydr. Polym.*, **221**, 146 (2019), <https://doi.org/10.1016/j.carbpol.2019.05.080>
- ²⁸ B. Wang, X. Lv, Z. Li, Y. Yao, Z. Yan *et al.*, *Cellulose*, **26**, 7411 (2019), <https://doi.org/10.1007/s10570-019-02602-x>
- ²⁹ K. Markstedt, A. Escalante, G. Toriz and P. Gatenholm, *ACS Appl. Mater. Interfaces*, **9**, 40878 (2017), <https://doi.org/10.1021/acsami.7b13400>
- ³⁰ R. J. Moon, A. Martini, J. Nairn, J. Simonsen and J. Youngblood, *Chem. Soc. Rev.*, **40**, 3941 (2011), <https://doi.org/10.1039/C0CS00108B>
- ³¹ T. Starborg, N. Kalson and Y. Lu, *Nat. Protoc.*, **8**, 1433 (2013), <https://doi.org/10.1038/nprot.2013.086>
- ³² N. T. Laçin, *Int. J. Biol. Macromol.*, **67**, 22 (2014), <https://doi.org/10.1016/j.ijbiomac.2014.03.003>
- ³³ B. Raphael, T. Khalil, V. L. Workman, A. Smith, C. P. Brown *et al.*, *Mater. Lett.*, **190**, 103 (2017), <https://doi.org/10.1016/j.matlet.2016.12.127>
- ³⁴ V. Karageorgiou and D. Kaplan, *Biomaterials*, **26**, 5474 (2005), <https://doi.org/10.1016/j.biomaterials.2005.02.002>
- ³⁵ H. Chen, A. de Botelho Ferreira Braga Malheiro, C. van Blitterswijk, C. Mota, P. A. Wieringa *et al.*, *ACS Appl. Mater. Interfaces*, **9**, 38187 (2017), <https://doi.org/10.1021/acsami.7b07151>
- ³⁶ I. Reiniati, A. N. Hrymak and A. Margaritis, *Crit. Rev. Biotechnol.*, **37**, 510 (2017), <https://doi.org/10.1080/07388551.2016.1189871>
- ³⁷ K. Fijałkowski, A. Żywicka, R. Drozd, A. F. Junka, D. Peitler *et al.*, *Electromagn. Biol. Med.*, **36**, 192 (2017), <https://doi.org/10.1080/15368378.2016.1243554>
- ³⁸ A. Salerno and P. A. Nettis, in “Biomedical Foams for Tissue Engineering Applications”, Elsevier, 2014, pp. 71-100, <https://doi.org/10.1533/9780857097033.1.71>
- ³⁹ S. Chawla, S. Midha, A. Sharma and S. Ghosh, *Adv. Healthc. Mater.*, **7**, 1701204 (2018), <https://doi.org/10.1002/adhm.201701204>
- ⁴⁰ C. Gao, Y. Z. Wan, C. X. Yang, K. R. Dai, T. T. Tang *et al.*, *J. Porous Mater.*, **18**, 139 (2011), <http://dx.doi.org/10.1007/s10934-010-9364-6>
- ⁴¹ J. Guo and J. M. Catchmark, *Carbohydr. Polym.*, **87**, 1026 (2012)
- ⁴² M. Ul-Islam, T. Khan and J. K. Park, *Carbohydr. Polym.*, **88**, 596 (2012)
- ⁴³ H. Barud, C. Ribeiro, M. Crespi, M. Martinez, J. Dexpert-Ghys *et al.*, *J. Therm. Anal. Calorim.*, **87**, 815 (2007), <https://doi.org/10.1007/s10973-006-8170-5>
- ⁴⁴ L. Segal, J. J. Creely, A. E. Martin and C. M. Conrad, *Text. Res. J.*, **29**, 786 (1959), <https://doi.org/10.1177/004051755902901003>
- ⁴⁵ A. Vazquez, M. L. Foresti, P. Cerrutti and M. Galvagno, *J. Polym. Environ.*, **21**, 545 (2013), <https://doi.org/10.1007/s10924-012-0541-3>
- ⁴⁶ F. V. Berti, C. R. Rambo, P. F. Dias and L. M. Porto, *Mater. Sci. Eng. C*, **33**, 4684 (2013), <https://doi.org/10.1016/j.msec.2013.07.029>